Elucidation of the Electronic Structure of Semiconducting Single-Walled Carbon Nanotubes by Electroabsorption Spectroscopy

Hongbo Zhao* and Sumit Mazumdar

Department of Physics, University of Arizona, Tucson, Arizona 85721, USA

(Received 23 January 2007; published 20 April 2007)

We report benchmark calculations of electroabsorption in semiconducting single-walled carbon nanotubes that provide motivation to perform electroabsorption measurement on these systems. We show that electroabsorption can detect the continuum bands in different energy manifolds. Direct determination of the binding energies of excitons in higher manifolds thereby becomes possible. We also find that electroabsorption can provide evidence for Fano-type coupling between the second exciton and the lowest continuum band states.

DOI: 10.1103/PhysRevLett.98.166805 PACS numbers: 73.22.−f, 71.35.−y, 78.67.Ch

Semiconducting single-walled carbon nanotubes (*S*-SWCNTs) are being intensively investigated because of their unique properties and broad potential for applications [1,2]. Recent theoretical investigations have emphasized the strong role of electron-electron interactions and the consequent excitonic energy spectra in *S*-SWCNTs [3–7]. While within one-electron theory two-photon absorption (TPA) begins at the same energy threshold as the lowest one-photon absorption, exciton theories predict a significant energy gap between the lowest two-photon exciton and the optical exciton [8,9]. This energy gap gives the lower bound to the binding energy of the lowest exciton and has been determined experimentally [8–11].

We note, however, that existing experiments have focused almost entirely on the lowest exciton, and information on the *overall energy spectra* of *S*-SWCNTs is severely limited. No signature of even the lowest continuum band is obtained from such experiments. Finite diameters of *S*-SWCNTs lead to subband quantization and a series of energy manifolds labeled $n = 1, 2, \ldots$, etc., with increasing energies (see Fig. 4 in Ref. [9]), and although emission studies detect the optical exciton in the $n = 2$ manifold ($Ex2$) [12], it has not been possible to determine its binding energy. TPA or transient absorption techniques used to determine the binding energy of the optical exciton in the $n = 1$ manifold ($Ex1$) are not useful for this, as nonlinear absorptions to states in the $n = 2$ manifold will be masked by the linear absorption to $Ex1$. Interference effects between $Ex2$ and the $n = 1$ continuum band, suggested from relaxation studies of $Ex2$ [13,14], are also difficult to verify directly. Clearly, measurements that can probe much broader energy regions of *S*-SWCNTs are called for.

In the present Letter, we propose electroabsorption (EA), which measures the difference between the absorption $\alpha(\omega)$ with and without an external static electric field, as the ideal technique for understanding the overall energy spectra of *S*-SWCNTs. EA has provided valuable information on both conventional semiconductors [15] and π-conjugated polymers [16–18]. The similarity in the energy spectra of π-conjugated polymers and *S*-SWCNTs [7,9] makes EA particularly attractive. EA spectroscopy of *S*-SWCNTs has already been attempted [19], while continuous wave photomodulation spectroscopy has been interpreted as electroabsorption caused by local electric fields [20]. EA measurements are currently difficult as complete separation of semiconducting from metallic SWCNTs has not been possible to date. Recent advances in the syntheses of chirality enriched *S*-SWCNTs [21] strongly suggest that EA measurements will become possible in select *S*-SWCNTs in the near future. We present here benchmark calculations of EA for several wide nanotubes that give new insights to their electronic structures and provide the motivation for and guidance to experimental work.

As in our previous work [7,9], we choose the semiempirical π-electron Pariser-Parr-Pople (PPP) model [22] as our field-free Hamiltonian,

$$H_0 = -\sum_{\langle ij\rangle,\sigma} t_{ij}(c^\dagger_{i\sigma}c_{j\sigma} + c^\dagger_{j\sigma}c_{i\sigma}) + U\sum_i n_{i\uparrow}n_{i\downarrow} + \frac{1}{2}\sum_{i\neq j} V_{ij}(n_i - 1)(n_j - 1). \quad (1)$$

Here, $c^\dagger_{i\sigma}$ creates a π-electron with spin σ on the ith carbon atom, $\langle ij\rangle$ implies nearest neighbors, $n_{i\sigma} = c^\dagger_{i\sigma}c_{i\sigma}$ is the number of π-electrons with spin σ on the atom i, and $n_i = \sum_\sigma n_{i\sigma}$. The parameter t_{ij} is the one-electron hopping integral, U is the repulsion between two π-electrons occupying the same carbon atom, and V_{ij} the intersite Coulomb interaction. We have chosen U, V_{ij}, and t_{ij} as in our recent work [7]. In principle, we should also include the electron-phonon interaction [6]. This, however, will make the EA calculations much too complicated. In agreement with prior EA experiments on π-conjugated polymers [16], our calculations here find that EA signals due to excitons and continuum bands are sufficiently different that there

can be no confusion in distinguishing between exciton sidebands and continuum bands.

We are interested in optical absorptions polarized parallel to the nanotube axis and consider only the component of the static electric field along the same direction. The overall Hamiltonian is written as [17]

$$H = H_0 + eFz = H_0 + \mu F, \tag{2}$$

where e is the charge of the electron, F the field strength along the nanotube axis (taken to be the z direction), and μ the transition dipole operator along z.

The EA is calculated in two steps [17]. We first diagonalize H_0 in the space of single excitations from the Hartree-Fock (H-F) ground state, using the single-configuration interaction (SCI) approximation [7]. While higher order correlation effects are certainly important, we have recently shown that with appropriate parametrization of Hamiltonian (1), it is possible to determine nearly quantitatively the exciton energies and exciton binding energies within the SCI for S-SWCNTs with diameters greater than 0.75 nm, the systems of interest here [7]. Eigenstates of S-SWCNTs are of even (A_g) or odd (B_u) parity, and dipole matrix elements are nonzero only between states of opposite parity [23]. We calculate the field-free absorption spectra $\alpha(\omega; 0)$ from the calculated dipole matrix elements between the ground state $1A_g$ and excited B_u states [7,9]. We now evaluate the matrix elements of μ between all excited states of H_0. A unique A_g exciton above $1B_u$ (or $Ex1$) that has very large dipole coupling with $1B_u$ is identified as the two-photon mA_g state [9,17] that is visible in TPA and transient absorption [8–10]. The nB_u, the threshold state of the $n = 1$ continuum, is similarly identified as the unique B_u state that occurs above mA_g and has very large dipole coupling with mA_g [17]. We construct and diagonalize the total Hamiltonian H with the eigenstates of H_0 as the basis states, and calculate the new absorption $\alpha(\omega; F)$. The EA is given by $\Delta\alpha(\omega; F) = \alpha(\omega; F) - \alpha(\omega; 0)$.

The effect of the nonzero field is to mix A_g and B_u states. Within second order perturbation theory appropriate for weak fields, $Ex1$ undergoes a Stark energy shift ΔE_{Ex1}, given by

$$\Delta E_{Ex1} = \sum_j \frac{|\langle Ex1|\mu|jA_g\rangle|^2 F^2}{E_{Ex1} - E_{jA_g}}. \tag{3}$$

In addition, A_g excitons that are forbidden for $F = 0$ become weakly allowed for $F \neq 0$. This transfer of oscillator strengths between A_g and B_u excitons is also quadratic in F. Nondegenerate perturbation theory cannot, however, describe the mixing of A_g and B_u states belonging to continuum bands, and the EA in these energy regions can be only calculated numerically. As we discuss below, the same is true for $Ex2$, which is buried within the $n = 1$ continuum. We do not discuss the dark excitons [6,7] separately, as they are not dipole coupled to the optical excitons. It is conceivable that the lowest dark exciton gets populated following rapid nonradiative decay from the optical exciton and takes part in nonlinear absorption [9]. However, the higher excited state that is dipole coupled to the dark exciton is energetically so close to mA_g (see Fig. 5 in [9]) that it will not be separately identifiable in the EA experiment.

We first describe the $n = 1$ energy region separately. In Fig. 1(a), we have plotted the calculated linear absorption along with EA spectrum in the energy range corresponding to the $n = 1$ manifold for $F = 10$ kV/cm for (10,0) NT. Figures 1(b)–1(d) show the EA spectra for $F = 50$, 100, and 200 kV/cm, respectively. EA for other S-SWCNTs, including chiral ones, are similar. The three most important features of the EA spectra are indicated in Fig. 1(a). The derivative-like feature A corresponds to the redshift of $Ex1$. The redshift (as opposed to a blueshift) is a consequence of (i) $|\langle mA_g|\mu|1B_u\rangle| > |\langle 1A_g|\mu|1B_u\rangle|$, and (ii) $E_{mA_g} - E_{1B_u} < E_{1B_u} - E_{1A_g}$. Feature B corresponds to the field-induced absorption to mA_g. Feature C is a dip in EA due to nB_u. The continuum band is recognized by its oscillatory nature, and its appearance over a broad energy region where there is no linear absorption. EA can therefore give the binding energy of $Ex1$ directly, as the energy difference between the features C and A.

The amplitude of the continuum band signal in Fig. 1 is much larger than that of the exciton at low field. This has been observed previously in a crystalline polydiacetylene [16]. Features due to the exciton and the continuum can be distinguished easily even when electron-phonon interactions lead to sidebands, from their different field dependence [16]. In Fig. 2(a), we show that the calculated field dependence of both $|\Delta E_{Ex1}|$ and the amplitude of EA signal due to $Ex1$ for (6,5), (7,6), and (10,0) NTs are quadratic in F up to the largest value of F. EA amplitudes due to nB_u, also plotted in the figure, exhibit weaker dependence on F at strong fields. In Figs. 2(b) and 2(c),

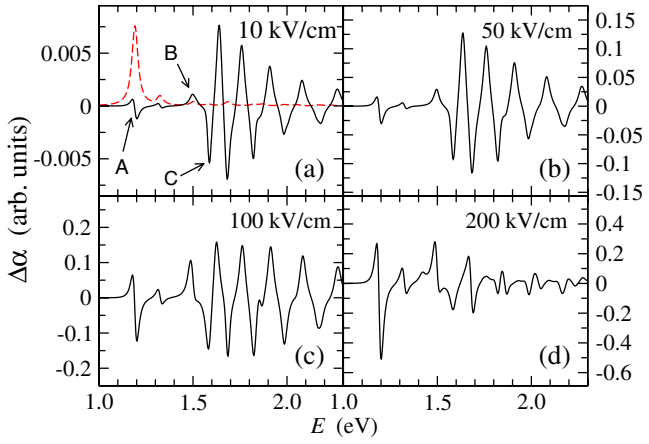

FIG. 1 (color online). (a) Linear absorption (dashed line), and EA spectrum of (10,0) NT in the $n = 1$ energy region for $F = 10$ kV/cm. (b)–(d) EA spectra for $F = 50$, 100, and 200 kV/cm, respectively.

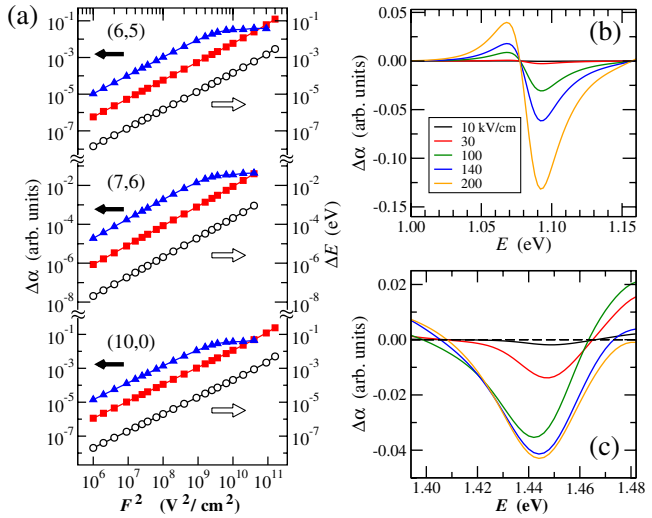

FIG. 2 (color online). (a) Field dependence of ΔE_{Ex1} (open circles), the EA amplitude of $Ex1$ (solid squares), and nB_u (solid triangles) for the (6,5), (7,6), and (10,0) S-SWCNTs. (b) and (c) Field dependence of EA signals for the (6,5) S-SWCNT due to the $Ex1$ and the nB_u, respectively.

we plotted EA signals due to $Ex1$ and nB_u, respectively, at different fields. EA due to the continuum (but not the exciton) exhibits the expected band broadening [16] as a function of the field.

We now discuss EA over the entire energy region, focusing on the $n = 2$ manifold. Figure 3(a) shows the calculated linear absorption for (6,5) NT, while Fig. 3(b) shows the EA spectrum for $F = 50$ kV/cm. The EA spectrum is dominated by two distinct oscillating signals due to the $n = 1$ and 2 continuum bands. The signal due to $Ex2$, which lies within the $n = 1$ continuum, is much stronger

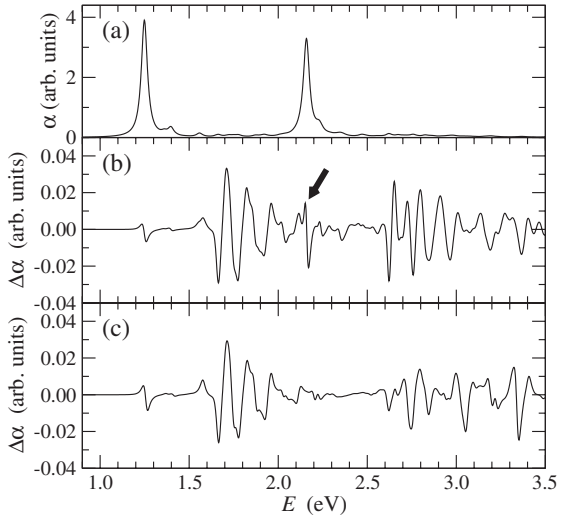

FIG. 3. Linear absorption (a) and EA spectrum (b) in the energy region covering both $n = 1$ and 2 energy manifolds for the (6,5) S-SWCNT for $F = 50$ kV/cm. The arrow indicates $Ex2$. (c) Superposition of the EAs for the $n = 1$ and 2 manifolds, calculated independently of one another.

than that due to $Ex1$. This is a consequence of the interference between $Ex2$ and the $n = 1$ continuum, as we prove by comparing the true EA of Fig. 3(b) with that in Fig. 3(c), where the coupling between $Ex2$ and the $n = 1$ continuum states has been artificially eliminated. We calculated EA from the $n = 1(2)$ manifold states separately by removing all $n = 2(1)$ states from Eq. (2). Figure 3(c) shows the superposition of these two independent EAs. The very small EA signal due to $Ex2$ in Fig. 3(c) is completely obliterated by the envelope of the $n = 1$ continuum, indicating that the much larger signal in Fig. 3(b) is a consequence of the coupling between $Ex2$ and the $n = 1$ continuum states. We have further verified this by performing the EA calculations with varying U/t: larger Coulomb interactions imply larger Coulomb coupling between $Ex2$ and the $n = 1$ continuum and give larger EA signal for $Ex2$. We have observed these characteristics in our calculated EA spectra for all S-SWCNTs.

Coulomb coupling between a discrete state with a continuum leads to the well-known Fano resonance, which manifests itself as a sharp asymmetric line in the linear absorption [24]. Calculation of the absorption spectrum of (8,0) NT has previously found this coupling [4]. In contrast to this standard description of the Fano effect, the interference effect we observe in the EA spectrum is a consequence of transition dipole coupling between $Ex2$ and the $n = 1$ continuum states. One interesting consequence of this dipole coupling is that $Ex2$ can be either redshifted [as observed in our calculations for (6,4), (7,6), and (11,0) NTs] or blueshifted [observed for (6,2), (8,0), and (10,0) NTs]. The reason for this is explained in Table I, where we have listed for (8,0) and (6,4) NTs the dominant transition dipole couplings between $Ex2$ and A_g states along with the energy differences between them. Among these states, only one is from the $n = 2$ manifold, which is the mA_g2 state, the equivalent of the mA_g state in the $n = 2$ manifold. All other states belong to the $n = 1$ continuum. The relatively large energy difference between mA_g2 and $Ex2$, comparable to that between mA_g and $Ex1$, indicates that the

TABLE I. Dominant transition dipole couplings between $Ex2$ and A_g states, as well as the corresponding energy differences. The mA_g2 state is labeled with an asterisk (*).

(n, m)	$\langle Ex2\|\mu\|jA_g\rangle/\langle Ex2\|\mu\|1A_g\rangle$	$E_{Ex2} - E_{jA_g}$ (eV)
(8,0)	8.31*	−0.423
	8.01	0.057
	6.22	−0.103
	1.22	0.073
(6,4)	15.3	0.049
	11.5	−0.051
	11.1	0.081
	9.64	−0.070
	9.45	−0.080
	6.62	−0.025
	6.45*	−0.402

TABLE II. Relative weights of H-F $n = 1$ excitations in the SCI $Ex2$ eigenstate of several S-SWCNTs.

	(8,0)	(10,0)	(6,2)	(6,4)	(6,5)	(7,6)	(9,2)
percentage	3%	2%	23%	12%	20%	33%	26%

energy shift of $Ex2$ is determined predominantly by the dipole-coupled $n = 1$ continuum states. States below (above) $Ex2$ contribute to blue (red) shifts, and the energy differences in Table I rationalize blueshifts (redshifts) in the (8,0) [(6,4)] NT. The magnitude of the energy shift of $Ex2$ in all cases is smaller than that of $Ex1$ because of partial cancellations, even as the amplitude of the EA signal of $Ex2$ is larger.

Correlated SCI eigenstates of the Hamiltonian (1) are superpositions of band-to-band excitations from the H-F ground state. Within tight-binding model as well as H-F theory, matrix elements of the component of the dipole moment along the tube axis are nonzero only for ''symmetric'' excitations, viz., from the highest valence band to the lowest conduction band, from the second highest valence band to the second lowest conduction band, etc., Hence, the strong dipole couplings between $Ex2$ and $n = 1$ continuum states necessarily imply that $Ex2$ contains basis vector components belonging to both $n = 1$ and $n = 2$ manifolds. This is precisely the signature of Fano coupling. Table II shows the relative weights of the $n = 1$ one electron–one hole excitations in the correlated $Ex2$ eigenstates of several S-SWCNTs. These contributions are chirality-dependent and reach as high as 30%.

The threshold of the $n = 2$ continuum is always detectable in our calculated EA spectra. Further confirmation of the band edge can come from measurements of its field-dependence, which is the same as for $n = 1$. Taken together with emission measurements that give the energy location of $Ex2$ [12], EA can then give the precise binding energy of $Ex2$.

In conclusion, we have performed benchmark calculations showing that EA measurements in S-SWCNTs can provide valuable information on their electronic structures that are difficult to obtain from other measurements. In particular, EA spectroscopy can detect both $n = 1$ and 2 continuum bands, which are easily differentiated from EA due to excitons. Precise binding energies of $Ex1$ and $Ex2$ can therefore be obtained. The predicted redshift of $Ex1$ would provide indirect evidence for the mA_g state detected in complementary nonlinear absorption measurements [8–11]. High resolution will also allow direct detection of mA_g. We find strong evidence for Fano-type coupling between $Ex2$ and $n = 1$ continuum states [13,14]. Syntheses of chirality enriched S-SWCNTs are allowing a variety of sophisticated spectroscopic measurements. Our results provide strong motivation for EA spectroscopy of S-SWCNTs. It is tempting to extend the current EA calculations to the $n = 3$ energy region. Although the $n = 3$ exciton is identifiable from linear absorption calculations, our calculations indicate that its coupling to the $n = 2$ continuum states is even stronger than that of $Ex2$ with the $n = 1$ continuum. The analysis of excitons and continuum bands become rather complicated at these high energies. Work is currently in progress along this direction.

This work was supported by No. NSF-DMR-0406604.

Note added.—After submitting this manuscript, we became aware of a recent publication that has also investigated EA theoretically [25].

*Current address: Department of Physics, University of Hong Kong, Hong Kong, China

[1] P. L. McEuen, M. S. Fuhrer, and H. Park, IEEE Trans. Nanotechnol. **1**, 78 (2002).
[2] J. Chen *et al.*, Science **310**, 1171 (2005).
[3] T. Ando, J. Phys. Soc. Jpn. **66**, 1066 (1997); **73**, 3351 (2004).
[4] C. D. Spataru *et al.*, Phys. Rev. Lett. **92**, 077402 (2004); Appl. Phys. A **78**, 1129 (2004).
[5] E. Chang *et al.*, Phys. Rev. Lett. **92**, 196401 (2004).
[6] V. Perebeinos *et al.*, Phys. Rev. Lett. **92**, 257402 (2004); **94**, 027402 (2005).
[7] H. Zhao and S. Mazumdar, Phys. Rev. Lett. **93**, 157402 (2004); Z. Wang, H. Zhao, and S. Mazumdar, Phys. Rev. B **74**, 195406 (2006).
[8] J. Maultzsch *et al.*, Phys. Rev. B **72**, 241402 (2005).
[9] H. Zhao *et al.*, Phys. Rev. B **73**, 075403 (2006).
[10] F. Wang *et al.*, Science **308**, 838 (2005).
[11] G. Dukovic *et al.*, Nano Lett. **5**, 2314 (2005).
[12] S. M. Bachilo *et al.*, Science **298**, 2361 (2002).
[13] C. Manzoni *et al.*, Phys. Rev. Lett. **94**, 207401 (2005).
[14] T. Hertel *et al.*, Phys. Status Solidi B **243**, 3186 (2006).
[15] D. E. Aspnes, Phys. Rev. **147**, 554 (1966); **153**, 972 (1967).
[16] G. Weiser and Á. Horváth, in *Primary Photoexcitations in Conjugated Polymers: Molecular Exciton versus Semiconductor Band Model*, edited by N. S. Sariciftci (World Scientific, Singapore, 1998), pp. 318–362.
[17] D. Guo *et al.*, Phys. Rev. B **48**, 1433 (1993).
[18] M. Liess *et al.*, Phys. Rev. B **56**, 15712 (1997).
[19] J. W. Kennedy *et al.*, cond-mat/0505071.
[20] C. Gadermaier *et al.*, Nano Lett. **6**, 301 (2006).
[21] M. S. Arnold *et al.*, Nature Nanotechnology **1**, 60 (2006); R. Krupk *et al.*, Science **301**, 344 (2003); V. W. Brar *et al.*, J. Nanosci. Nanotech. **5**, 209 (2005).
[22] R. Pariser and R. G. Parr, J. Chem. Phys. **21**, 466 (1953); J. A. Pople, Trans. Faraday Soc. **49**, 1375 (1953).
[23] This is only approximately true for chiral NTs, but in practice there is no difference between zigzag and chiral; see Ref. [7].
[24] U. Fano, Phys. Rev. **124**, 1866 (1961).
[25] V. Perebeinos and Ph. Avouris, Nano Lett. **7**, 609 (2007).